Gluino Polarization at the LHC

M. Krämer[1], E. Popenda[1], M. Spira[2], and P. M. Zerwas[3,1]

[1] *Institut für Theoretische Physik E, RWTH Aachen University, D-52074 Aachen, Germany*
[2] *Paul Scherrer Institut, CH-5232 Villigen PSI, Switzerland*
[3] *Deutsches Elektronen-Synchrotron DESY, D-22603 Hamburg, Germany*

(Dated: February 22, 2009)

Gluinos are produced pairwise at the LHC in quark-antiquark and gluon-gluon collisions: $q\bar{q}, gg \to \tilde{g}\tilde{g}$. While the individual polarization of gluinos vanishes in the limit in which the small mass difference between L and R squarks of the first two generations is neglected, non-zero spin-spin correlations are predicted within gluino pairs. If the squark/quark charges in Majorana gluino decays are tagged, the spin correlations have an impact on the energy and angular distributions in reconstructed final states. On the other hand, the gluino polarization in single gluino production in the supersymmetric Compton process $gq \to \tilde{g}\tilde{q}_{R,L}$ is predicted to be non-zero, and the polarization affects the final-state distributions in super-Compton events.

1. INTRODUCTION

Gluinos in the Minimal Supersymmetric Standard Model [MSSM] [1, 2, 3] can be produced copiously at the LHC, *cf.* Refs. [4, 5]; gluino pairs in quark-antiquark and gluon-gluon collisions, Figs. 1(a/b),

$$q\bar{q} \to \tilde{g}\tilde{g} \tag{1.1}$$

$$gg \to \tilde{g}\tilde{g}, \tag{1.2}$$

and single gluinos in association with squarks in the super-Compton process, Fig. 1(c),

$$qg \to \tilde{q}\tilde{g}. \tag{1.3}$$

After the gluinos decay, the final-state energy and angular distributions will in general depend on the degree of polarization with which the gluinos are generated.[1] Thus the distribution of experimentally reconstructed events is affected by the polarization of the gluinos.

However, polarization effects are to a large extent expunged by the Majorana character of the particles, in particular when parton charges are not measured. For example, jet angular distributions in[2]

$$\tilde{g} \to q_{R,L}\, \tilde{q}_{R,L}^* \quad \text{and} \quad \tilde{g} \to \bar{q}_{L,R}\, \tilde{q}_{R,L} \tag{1.4}$$

follow, mutually, the $[1 \pm \cos\theta]$ law with regard to the gluino spin vector so that the sum of the spin-dependent terms vanishes, as a result of CP-invariance if $q, \tilde{q}$ charges are not analyzed. [For the sake of simplicity we will restrict ourselves to the class of SPS1a/a′-type scenarios [7] in which the gluinos are heavier than the squarks so that the complexity of gluino decay patterns is reduced to the maximum extent possible.]

If gluinos, on the other hand, were Dirac particles $\tilde{g}_D$ as may be formalized in N=2 hybrid models [8, 9, 10, 11], the conservation of the Dirac charge D, with $D = +1$ for $\tilde{g}_D, \tilde{q}_R$ and -1 for $\tilde{g}_D^c, \tilde{q}_L$ [8], allows only the production

---

[1] Spin measurements of supersymmetric particles *sui generis* at the LHC are widely discussed in the literature; for a sample of methods that address the impact of spin on differential distributions see Ref. [6].
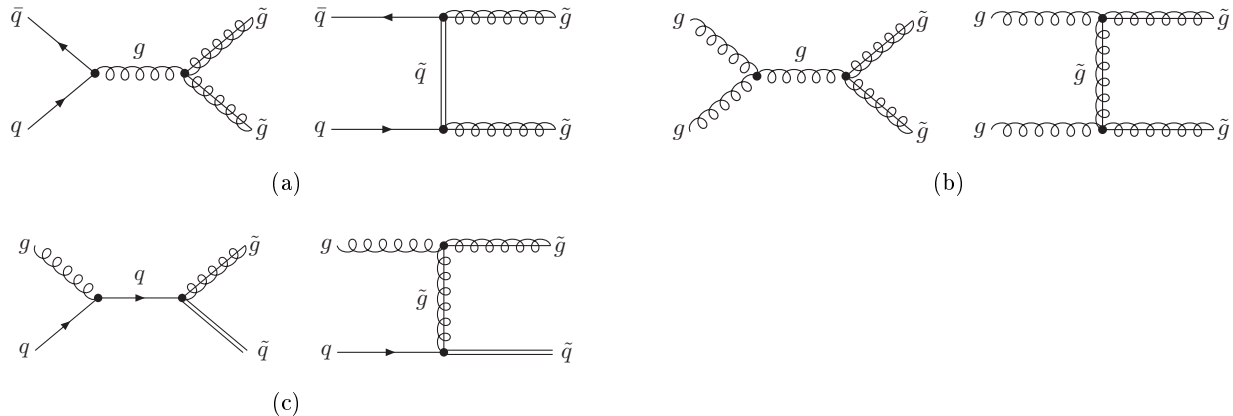[2] The indices R,L denote the $\pm$ helicities of quarks and antiquarks.

FIG. 1: Feynman diagrams for gluino production in quark annihilation (a), gluon fusion (b) and in the super-Compton process (c).

of specific pairs of supersymmetric particles and antiparticles: $\tilde{g}_D \tilde{g}_D^c$; $\tilde{g}_D \tilde{q}_L$, $\tilde{g}_D^c \tilde{q}_R$ *etc.*, followed by specific decay patterns: $\tilde{g}_D \to q_L \tilde{q}_L^*$ *but not* $\tilde{g}_D \to \bar{q}_R \tilde{q}_L$, and crosswise for R-squarks/anti-squarks. This gives rise to stringent restrictions on polarization and spin-correlation effects. Observing or not observing such correlations thus signals the Dirac/Majorana character of gluinos.

1) Gluino pairs: The masses of L and R-squarks of the first two generations are generally close to each other. Neglecting the small mass differences, the super-QCD action of the first two generations becomes invariant under P-transformation combined with the exchange of $\tilde{q}_L \leftrightarrow \tilde{q}_R$. As a result, the single polarization of gluinos vanishes in the pair production processes (1.1) and (1.2). However, spin correlations within the gluino pair are non-trivial.

As argued before, the sum of polarization asymmetries adds up to zero in CP-invariant theories, if the charges are not measured in the gluino decay modes. Hence, the jets which originate in equal shares from quarks and antiquarks in (1.4) are isotropically distributed. The distribution in the scaled jet-jet mass, $m = 2M_{jj}/\sqrt{s}$ in the decay $\tilde{g}\tilde{g} \to qq' + X$ is then moderately soft,

$$\text{isotropic}: \quad \sigma^{-1} d\sigma/dm^2 = \log m^{-2} \tag{1.5}$$

for asymptotic energies $s \gg M_{\tilde{g}}^2 \gg M_{\tilde{q}}^2$ [6, 12]. However, charges can be tagged in $\tilde{u}_L, \tilde{d}_L$ decays to charginos, $\tilde{q}_L \to q\tilde{\chi}_1^{\pm} \to ql^{\pm}\nu_l\tilde{\chi}_1^0$. This is useful in scenarios in which $\tilde{\chi}_2^0$ is not a pure wino or bino state so that the branching ratios of $\tilde{u}_L$ and $\tilde{d}_L^*$ are different. In such scenarios polarization effects do not completely cancel among the decay chains $\tilde{g} \to \bar{u}_R \tilde{u}_L \to \bar{u}_R d\tilde{\chi}_1^+$ and $\tilde{g} \to d_L \tilde{d}_L^* \to d_L \bar{u}\tilde{\chi}_1^+$, which result in identical final state charges, but have opposite polarization signatures. Tagging of top and bottom charges in the third generation can be exploited in any case. In the asymptotic limit in which gluino fragmentation to quarks [plus accompanying squarks] is either hard or soft, *i.e.* $\sim 2z$ or $2(1-z)$ for quarks emitted preferentially parallel or anti-parallel to the gluino spin, various configurations can be realized for the invariant mass distributions of the near-jet pairs[3] in $\tilde{g}\tilde{g} \to qq' + X$ final states [12]:

$$\begin{aligned}
\text{hard} - \text{hard}: \quad \sigma^{-1} d\sigma/dm^2 &= 4m^2 \log m^{-2} \\
\text{hard} - \text{soft}: \quad &= 4\left[(1 - m^2) - m^2 \log m^{-2}\right] \\
\text{soft} - \text{soft}: \quad &= 4\left[(1 + m^2)\log m^{-2} - 2(1 - m^2)\right].
\end{aligned} \tag{1.6}$$

The four mass distributions are compared with each other in Fig. 2(a). Evidently, the gluino polarization leads to distinct patterns in the invariant jet-jet distributions.

---

[3] The far-jets will be taken into account properly in the detailed phenomenology subsections.
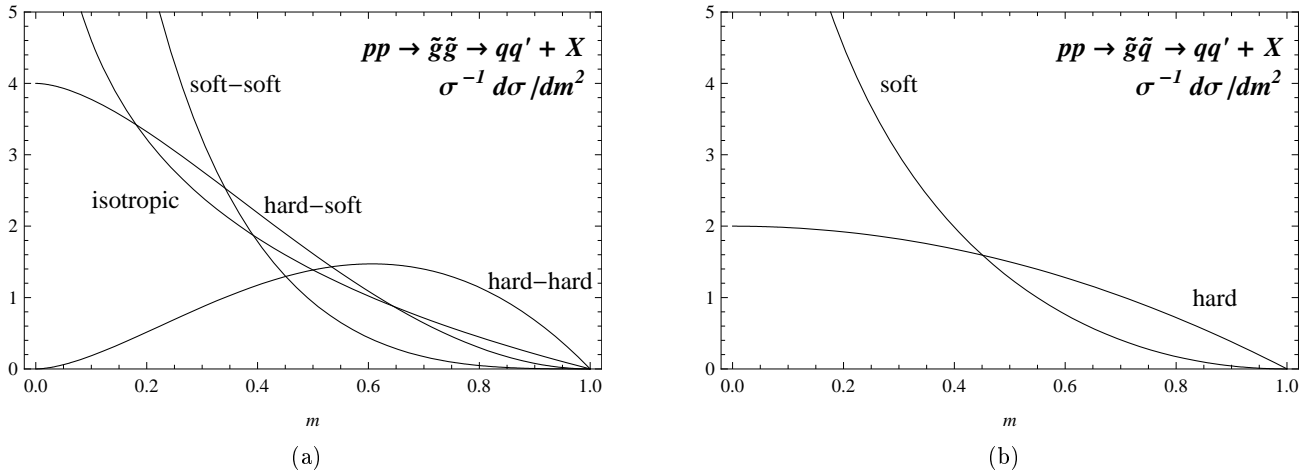
FIG. 2: Invariant near-jet jet mass distributions in the gluino pair production processes (a) and the super-Compton process (b) for various combinations of hard and soft fragmentation $\tilde{g} \to q$.

If no charges are measured, the MSSM Majorana theory predicts the moderately soft mass distribution Eq. (1.5) of the near-quark jets in the gluino decays. In a gluino Dirac theory, on the other hand, pairs $\tilde{g}_D \tilde{g}_D^c$ are generated decaying to $\tilde{q}_L \tilde{q}_L^*$ *but not* $\tilde{q}_L \tilde{q}_L$ final states [8]. Such a theory would therefore predict an invariant mass distribution of the hard-hard and soft-soft types for aligned gluino spins. Thus, the shape of the mass distributions discriminates between standard Majorana and other Dirac supersymmetric theories.

2) Super-Compton process: Since the processes Eq. (1.3) are maximally P-violating if L and R-squarks are discriminated by their decay patterns, the produced gluinos are polarized. The polarization can be measured by exploiting the same methods for the first two and the third generation as outlined above. The polarization reflects itself in the invariant mass distribution of the near-quark jet in the gluino cascade with the primary squark decay jet, for asymptotic energies:

$$\begin{aligned}
\text{hard}: \quad \sigma^{-1} d\sigma/dm^2 &= 2\,(1 - m^2) \\
\text{soft}: \quad &= 2\left[\log m^{-2} - (1 - m^2)\right].
\end{aligned} \tag{1.7}$$

The two distributions are displayed in Fig. 2(b), exhibiting quite different shapes for the hard and soft decay configurations.

Switching from Majorana to Dirac gluinos does not affect the degree of gluino polarization. Nevertheless, as a result of D-conservation $\tilde{g}_D$ states are generated only in association with $\tilde{q}_L$ states, and $\tilde{g}_D^c$ states only in association with $\tilde{q}_R$ states, and cc pairs correspondingly [8]. The decays of the $\tilde{g}_D^{(c)}$ particles follow the pattern discussed earlier.

The report includes two central sections. In Section 2 we analyze spin-spin correlations in gluino pair production, followed by the discussion of the super-Compton process in Section 3. In both sections we present analytical results at the parton level, and we illustrate the spin effects by calculating jet-jet invariant mass distributions for gluino production and decay at the LHC. While only the basic theoretical points are elaborated to emphasize the salient features of the spin correlations, the analysis nevertheless demonstrates the potential impact of spin-correlations for high-precision supersymmetry studies at the LHC in the future. Section 4 concludes the report.

2. GLUINO POLARIZATION IN PAIR PRODUCTION

2.1. Gluino Production at the Parton Level

The s and t-channel exchange mechanisms, complimented by the u-channel exchanges, are shown in Figs. 1(a) and (b) for quark-antiquark and gluon-gluon collisions. For unpolarized beams the parton-parton cross sections are given by [4, 5]

$$\sigma[q\bar{q} \to \tilde{g}\tilde{g}] = \frac{\pi\alpha_s^2}{s}\beta\left(\frac{8}{9} + \frac{4m_{\tilde{g}}^2}{9}\right) - \frac{\pi\alpha_s\hat{\alpha}_s}{s}\left[\left(\frac{2m_{\tilde{g}}^2}{3} + \frac{m_-^4}{6}\right)L + \beta\left(\frac{4}{3} + \frac{2m_-^2}{3}\right)\right]$$
$$+ \frac{\pi\hat{\alpha}_s^2}{s}\left[\left(\frac{16m_-^2}{27} + \frac{4m_{\tilde{g}}^2}{27\left(2 - m_-^2\right)}\right)L + \beta\left(\frac{32}{27} + \frac{32m_-^4}{27\left(4m_{\tilde{q}}^2 + m_-^4\right)}\right)\right]$$

$$\sigma[gg \to \tilde{g}\tilde{g}] = \frac{\pi\alpha_s^2}{s}\left[\left(\frac{9}{4} + \frac{9m_{\tilde{g}}^2}{4} - \frac{9m_{\tilde{g}}^4}{16}\right)\log\left(\frac{1+\beta}{1-\beta}\right) - \beta\left(3 + \frac{51m_{\tilde{g}}^2}{16}\right)\right] \tag{2.1}$$

where

$$L = \log\frac{1 + \beta - m_-^2/2}{1 - \beta - m_-^2/2} \quad\text{with}\quad \beta = \sqrt{1 - m_{\tilde{g}}^2}\,,$$

$$\alpha_s = g_s^2/4\pi \quad\text{and}\quad \hat{\alpha}_s = \hat{g}_s^2/4\pi\,,$$

if the polarization of the gluinos in the final state is not measured. All masses are scaled by the parton beam energy $\sqrt{s}/2$ in the parton-parton c.m. frame, i.e.

$$m_{\tilde{g},\tilde{q}} = 2M_{\tilde{g},\tilde{q}}/\sqrt{s} \quad\text{and}\quad m_- = 2\sqrt{|M_{\tilde{g}}^2 - M_{\tilde{q}}^2|/s}\,. \tag{2.2}$$

The couplings g_s and $\hat{g}_s$ are the QCD gauge and Yukawa couplings, respectively, which are identical in super-QCD. Though noted here in Born approximation [4], the cross sections are known more accurately at next-to-leading order in super-QCD [5] and including threshold resummations [13]. The angular distributions for gluino pair production read:

$$\frac{d\sigma}{d\Omega}[q\bar{q} \to \tilde{g}\tilde{g}] = \frac{\beta}{s}\left[\frac{\alpha_s^2}{6}\left(2 + m_{\tilde{g}}^2 - \kappa_+\kappa_-\right) + \frac{2\alpha_s\hat{\alpha}_s}{3}\frac{m_{\tilde{g}}^2 + \kappa_+^2}{m_-^2 - 2\kappa_+}\right.$$
$$\left.+ \hat{\alpha}_s^2\left(\frac{32}{27}\frac{\kappa_+^2}{(m_-^2 - 2\kappa_+)^2} + \frac{4}{32}\frac{m_{\tilde{g}}^2}{(m_-^2 - 2\kappa_+)(m_-^2 - 2\kappa_-)}\right)\right]^{\mathcal{S}}$$

$$\frac{d\sigma}{d\Omega}[gg \to \tilde{g}\tilde{g}] = \frac{\alpha_s^2\beta}{s}\frac{9}{32}\left[\frac{\kappa_+^2\kappa_-^2 - 2m_{\tilde{g}}^2(m_{\tilde{g}}^2 - 1)}{2\kappa_+\kappa_-} + 2\frac{\kappa_+\kappa_- - m_{\tilde{g}}^2(m_{\tilde{g}}^2 - \kappa_+)}{\kappa_+^2} - \frac{2\kappa_+\kappa_- + (\kappa_+ - \kappa_-)m_{\tilde{g}}^2}{2\kappa_+}\right]^{\mathcal{S}}. \tag{2.3}$$

We use the definitions

$$\kappa_\pm = 1 \pm \beta\cos\theta$$
$$[F]^{\mathcal{S}/\mathcal{A}} = F(\cos\theta) \pm F(-\cos\theta)\,. \tag{2.4}$$

from this point on. The polar angle θ denotes the gluino flight direction with respect to the incoming particle momenta in the parton-parton c.m. frame. The angular distribution is forward-backward symmetric for the production of Majorana pairs. For the sake of brevity, the cross sections Eq. (2.3) will be denoted in the following by $\mathcal{N}_{q\bar{q}}$ and $\mathcal{N}_{gg}$ for the $q\bar{q}$ and gg channels, respectively.

Quite generally, non-trivial polarization effects are generated in super-QCD introduced by the parity violating quark-squark-gluino Yukawa couplings, while spin-spin correlations among the final-state gluinos are generated also by parity conserving gluon-gluino-gluino interactions. However, parity-violating effects in the first two generations of super-QCD are strongly suppressed by the small differences between the squark masses. In fact, the super-QCD action is invariant under the P-transformation supplemented by L/R-squark exchange in the limit of equal-mass L/R squarks. Since the modulus of the potential gluino polarization vector $|M_L^2 - M_R^2|/[M_L^2 + M_R^2] \sim 10^{-2}$ is expected to be small [14], we neglect these effects in the present analysis.

Spin-spin correlations are conveniently described by the tensor $\mathcal{C}_{\mu\nu}$ following the formalism developed in Ref. [15]:

$$\frac{d\sigma(s_1, s_2)}{d\Omega} = \frac{d\sigma}{d\Omega} \frac{1}{4} \left[1 + \mathcal{C}_{\mu\nu} s_1^\mu s_2^\nu \right] . \tag{2.5}$$

The two gluinos in the parton-parton c.m. frame are assigned the spin vectors s_1 and s_2; they are related to the spin vectors $\check{s}_{1,2}$ in the gluino rest frames by respective Lorentz transformations $s_{1,2} = \Lambda_{1,2} \check{s}_{1,2}$, the corresponding matrix $\check{\mathcal{C}}$ associated with the general spin-density matrix, see e.g. [16]. Choosing the $\hat{z}$-axis along one of the gluino flight directions, the $\hat{x}$-axis transverse to this vector within the production plane and pointing into the obtuse wedge between initial and final-state momenta, and the $\hat{y}$-axis normal to the production plane, the longitudinal, transverse and normal spin vectors can be written as

$$\begin{aligned} s_{1,2}^l &= [\beta, 0, 0, \pm 1] / m_{\tilde{g}} \\ s_{1,2}^t &= [0, \pm 1, 0, 0] \\ s_{1,2}^n &= [0, 0, \pm 1, 0] . \end{aligned} \tag{2.6}$$

The longitudinal $\pm$ components describe helicity $+$ states of the two gluinos; the spin vectors of the helicity $-$ states are given by $-s_{1,2}^l$. The matrix $\mathcal{C}$ is effectively $2 \times 2 \oplus 1 \times 1$ dimensional; it is symmetric for Majorana gluinos and consists of four non-trivial components: $ll, lt = tl, tt; nn$. Based on the correlation tensor, before orthogonalization with respect to the gluino momenta,

$$\begin{aligned} q\bar{q} \text{ channel}: \quad \mathcal{C}_{\mu\nu} &= \frac{\beta}{s} \left[\frac{\alpha_s^2}{6} \left(\beta^2 \sin^2\theta g_{\mu\nu} - 2\kappa_+ k_{1,\mu} k_{2\nu} \right) \right. \\ &+ \frac{\alpha_s \hat{\alpha}_s}{3} \frac{2\beta^2 \sin^2\theta g_{\mu\nu} - (m_{\tilde{g}}^2 + 2\kappa_-) k_{2\mu} k_{1\nu} + (m_{\tilde{g}}^2 - 2\kappa_+) k_{1\mu} k_{2\nu}}{m_-^2 - 2\kappa_+} \\ &\left. - \hat{\alpha}_s^2 \left(\frac{32}{27} \frac{m_{\tilde{g}}^2 k_{2\mu} k_{1\nu}}{(m_-^2 - 2\kappa_+)^2} - \frac{4}{27} \frac{\beta^2 \sin^2\theta g_{\mu\nu} + (m_{\tilde{g}}^2 - 2\kappa_+) k_{1\mu} k_{2\nu}}{(m_-^2 - 2\kappa_-)(m_-^2 - 2\kappa_+)} \right) \right]^{\mathcal{S}} / \mathcal{N}_{q\bar{q}} \end{aligned}$$

$$\begin{aligned} gg \text{ channel}: \quad \mathcal{C}_{\mu\nu} &= \frac{\alpha_s^2 \beta}{s} \frac{9}{32} \left[\frac{1}{2} \left(-\kappa_+ \kappa_- g_{\mu\nu} + 2\kappa_+ k_{1\mu} k_{2\nu} \right) \right. \\ &+ \frac{2m_{\tilde{g}}^2}{\kappa_+^2} \left((m_{\tilde{g}}^2 - \kappa_+) g_{\mu\nu} + k_{2\mu} k_{1\nu} \right) + \frac{1}{\kappa_+ \kappa_-} \left((m_{\tilde{g}}^4 + \beta^2 \sin^2\theta) g_{\mu\nu} + (m_{\tilde{g}}^2 - 2\kappa_+) k_{1\mu} k_{2\nu} \right) \\ &\left. + \frac{1}{2\kappa_+} \left(2(\kappa_+ \kappa_- + m_{\tilde{g}}^2 \beta \cos\theta) g_{\mu\nu} + (m_{\tilde{g}}^2 - 2\kappa_+) k_{1\mu} k_{2\nu} - (m_{\tilde{g}}^2 + 2\kappa_-) k_{2\mu} k_{1\nu} \right) \right]^{\mathcal{S}} / \mathcal{N}_{gg} \quad (2.7) \end{aligned}$$

with $[F]_{\mu\nu}^{\mathcal{S}}$ denoting the symmetrized tensor

$$[F]_{\mu\nu}^{\mathcal{S}} = F_{\mu\nu}(\cos\theta, k_1, k_2) + F_{\mu\nu}(-\cos\theta, k_2, k_1) , \tag{2.8}$$

and k_1, k_2 being the initial parton 4-momenta, the spin matrix-elements can easily be derived:

$$q\bar{q} \text{ channel}: \quad \mathcal{C}^{ll} = -\frac{\beta}{s}\left[\frac{\alpha_s^2}{6}\left(\beta^2 + (1 + m_{\tilde{g}}^2)\cos^2\theta\right) + \frac{2\,\alpha_s\hat{\alpha}_s}{3}\frac{\beta^2 + 2\beta\cos\theta + (1 + m_{\tilde{g}}^2)\cos^2\theta}{m_-^2 - 2\kappa_+}\right.$$

$$\left.+\hat{\alpha}_s^2\left(\frac{32}{27}\frac{(\beta + \cos\theta)^2}{(m_-^2 - 2\kappa_+)^2} + \frac{4}{27}\frac{m_{\tilde{g}}^2\cos^2\theta}{(m_-^2 - 2\kappa_-)(m_-^2 - 2\kappa_+)}\right)\right]^{\mathcal{S}}/\mathcal{N}_{q\bar{q}}$$

$$\mathcal{C}^{lt} = \frac{\beta m_{\tilde{g}}}{s}\sin\theta\left[\frac{\alpha_s^2}{3}\cos\theta + \frac{2\,\alpha_s\hat{\alpha}_s}{3}\frac{\beta + 2\cos\theta}{m_-^2 - 2\kappa_+}\right.$$

$$\left.+\hat{\alpha}_s^2\left(\frac{32}{27}\frac{\beta + \cos\theta}{(m_-^2 - 2\kappa_+)^2} + \frac{4}{27}\frac{\cos\theta}{(m_-^2 - 2\kappa_+)(m_-^2 - 2\kappa_-)}\right)\right]^{\mathcal{A}}/\mathcal{N}_{q\bar{q}}$$

$$\mathcal{C}^{tt} = -\frac{\beta}{s}\sin^2\theta\left[\frac{\alpha_s^2}{6}(m_{\tilde{g}}^2 + 1) + \frac{2\alpha_s\hat{\alpha}_s}{3}\frac{m_{\tilde{g}}^2 + 1}{m_-^2 - 2\kappa_+}\right.$$

$$\left.+\hat{\alpha}_s^2\left(\frac{32}{27}\frac{m_{\tilde{g}}^2}{(m_-^2 - 2\kappa_+)^2} + \frac{4}{27}\frac{1}{(m_-^2 - 2\kappa_-)(m_-^2 - 2\kappa_+)}\right)\right]^{\mathcal{S}}/\mathcal{N}_{q\bar{q}}$$

$$\mathcal{C}^{nn} = \frac{\beta^3}{s}\sin^2\theta\left[\frac{\alpha_s^2}{6} + \frac{2\,\alpha_s\hat{\alpha}_s}{3}\frac{1}{m_-^2 - 2\kappa_+} + \frac{4\,\hat{\alpha}_s^2}{27}\frac{1}{(m_-^2 - 2\kappa_+)(m_-^2 - 2\kappa_-)}\right]^{\mathcal{S}}/\mathcal{N}_{q\bar{q}} \quad (2.9)$$

$$gg \text{ channel}: \quad \mathcal{C}^{ll} = \frac{9\alpha_s^2\beta}{32m_{\tilde{g}}^2 s}\left[\kappa_+(\beta - \cos\theta)^2 - \frac{\kappa_+\kappa_-}{2}(1 + \beta^2) + \frac{2m_{\tilde{g}}^2}{\kappa_+^2}\left((\beta + \cos\theta)^2 + (1 + \beta^2)(m_{\tilde{g}}^2 - \kappa_+)\right)\right.$$

$$-\frac{1}{\kappa_+\kappa_-}\left((2\kappa_- - m_{\tilde{g}}^2)(\beta + \cos\theta)^2 - (1 + \beta^2)(m_{\tilde{g}}^4 + \beta^2\sin^2\theta)\right)$$

$$+\frac{1}{2\kappa_+}\left((m_{\tilde{g}}^2 - 2\kappa_+)(\beta - \cos\theta)^2 - (m_{\tilde{g}}^2 + 2\kappa_-)(\beta + \cos\theta)^2\right.$$

$$\left.\left.+2\,(1 + \beta^2)(\beta m_{\tilde{g}}^2\cos\theta + \kappa_+\kappa_-))\right]^{\mathcal{S}}/\mathcal{N}_{gg}$$

$$\mathcal{C}^{lt} = -\frac{9\alpha_s^2\beta}{32s}\frac{\sin\theta}{m_{\tilde{g}}}\left[\kappa_-(\beta + \cos\theta) + \frac{2m_{\tilde{g}}^2}{\kappa_+^2}(\beta + \cos\theta)\right.$$

$$\left.-\frac{1}{\kappa_+\kappa_-}(\beta + \cos\theta)(2\kappa_- - m_{\tilde{g}}^2) - \frac{m_{\tilde{g}}^2}{\kappa_+}(\beta + 2\cos\theta)\right]^{\mathcal{A}}/\mathcal{N}_{gg}$$

$$\mathcal{C}^{tt} = \frac{9\alpha_s^2\beta}{32s}\left[\kappa_+(\sin^2\theta - \frac{\kappa_-}{2}) + \frac{2m_{\tilde{g}}^2}{\kappa_+^2}(m_{\tilde{g}}^2 + \sin^2\theta - \kappa_+) - \frac{1}{\kappa_+\kappa_-}\left((2\kappa_+ - 1)\sin^2\theta - m_{\tilde{g}}^4\right)\right.$$

$$\left.+\frac{1}{\kappa_+}(\beta\,m_{\tilde{g}}^2\cos\theta + \kappa_+\kappa_- - 2\sin^2\theta)\right]^{\mathcal{S}}/\mathcal{N}_{gg}$$

$$\mathcal{C}^{nn} = -\frac{9\alpha_s^2\beta}{32s}\left[\frac{\kappa_+\kappa_-}{2} - \frac{2\,m_{\tilde{g}}^2(m_{\tilde{g}}^2 - \kappa_+)}{\kappa_+^2} - \frac{m_{\tilde{g}}^4 + \beta^2\sin^2\theta}{\kappa_+\kappa_-} - \frac{\kappa_+\kappa_- + m_{\tilde{g}}^2\beta\cos\theta}{\kappa_+}\right]^{\mathcal{S}}/\mathcal{N}_{gg}. \quad (2.10)$$

The index l denotes positive gluino helicity. The four correlation matrix elements are displayed for $\sqrt{s} = 2$ TeV and SPS1a$'$ masses $M_{\tilde{g}} = 607$ GeV and $M_{\tilde{q}} = M_{\tilde{u}_L} = 565$ GeV [7] in Figs. 3(a) and (b) in the $q\bar{q}$ and gg channels, respectively. The antisymmetric terms drop out if $q\bar{q}\oplus\bar{q}q$ channels are summed up for the symmetric pp kinematics. As expected, $\mathcal{C}^{ll}$, corresponding to $S_z = 0$ for two equal gluino helicities in $q\bar{q} \to \tilde{g}\tilde{g}$, approaches -1 for forward/backward production, lifted [in particular by means of the t/u-exchange $\tilde{u}, \tilde{d}$ propagators] to larger values in between for non-zero gluino masses. $\mathcal{C}^{tt}$, on the other hand, is maximal for perpendicular production. The correlation of the normal polarizations is negative for non-zero production angles but, as in the transverse direction, approaches zero for forward
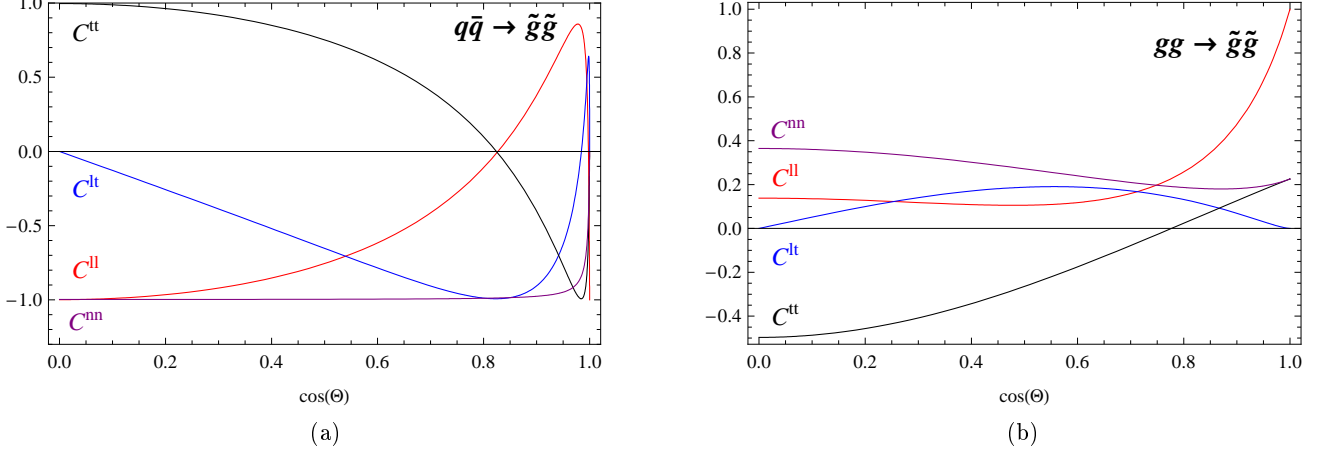
FIG. 3: Correlation matrix elements for $\sqrt{s} = 2$ TeV in the quark annihilation (a) and gluon fusion (b) channels.

production. The $S_z = 0$ component of the gluon-gluon spin wave-function in $gg \to \tilde{g}\tilde{g}$ gives rise to maximal forward production of $S_z = 0$ gluino pairs and, as expected, $\mathcal{C}^{tt}$ and $\mathcal{C}^{nn}$ approach equal values for forward production.

2.2. Gluino Decays

If gluinos are heavier than squarks, they decay to quarks and squarks [17]. The squarks decay subsequently to quarks plus neutralinos or charginos. Particularly at the reference point SPS1a/a$'$ the lightest neutralino $\tilde{\chi}_1^0$ is almost a pure bino state, while $\tilde{\chi}_2^0$ is almost a pure wino state, like the chargino $\tilde{\chi}_1^\pm$. The heavier neutralinos and charginos are higgsino-like states, and they do not play a significant role for matter particles of the first two generations. R-squarks will therefore decay predominantly into the lightest neutralino $\tilde{\chi}_1^0$ as LSP, while L-sqarks decay preferentially to the heavier neutralino $\tilde{\chi}_2^0$ or chargino $\tilde{\chi}_1^\pm$, followed by subsequent $\tilde{\chi}$ cascades. The decay branching ratios [18] are collected in the following set for the reference point SPS1a$'$:

$$\begin{aligned}
\Gamma[\tilde{g} \to q\tilde{q}_L] &= 7.73\% & \Gamma[\tilde{g} \to q\tilde{q}_R] &= 17.0\% & q \neq b, t \\
\Gamma[\tilde{g} \to b\tilde{b}_1] &= 10.8\% & \Gamma[\tilde{g} \to b\tilde{b}_2] &= 4.67\% & \\
\Gamma[\tilde{g} \to t\tilde{t}_1] &= 9.81\% \, .
\end{aligned} \tag{2.11}$$

The decay $\tilde{g} \to t\tilde{t}_2$ is kinematically forbidden.

If the gluinos are polarized along the axis $\vec{s}$ in the rest frame, final-state distributions are determined by the polarization vector $\mathcal{P}_\mu$,

$$d\Gamma = d\Gamma^{\mathrm{unpol}}\left[1 - \mathcal{P}_\mu s_\mu\right], \tag{2.12}$$

in a general Lorentz frame $\check{s}_\mu \to s_\mu$.

For gluinos polarized with degree unity, the angular distribution of the quark jets with respect to the spin axis depends on the particle/antiparticle character of the squarks, for the first two generations:

$$\begin{aligned}
\frac{1}{\Gamma}\frac{d\Gamma}{d\cos\theta}[\tilde{g} \to q_{R,L}\,\tilde{q}_{R,L}^*] &= \frac{1}{2}\left[1 \pm \cos\theta\right] \\
\frac{1}{\Gamma}\frac{d\Gamma}{d\cos\theta}[\tilde{g} \to \bar{q}_{L,R}\,\tilde{q}_{R,L}] &= \frac{1}{2}\left[1 \mp \cos\theta\right] .
\end{aligned} \tag{2.13}$$

The mass eigenstates of sparticles of the third generation, stop particles in particular, are mixtures of R,L current eigenstates [19] . Denoting the $\tilde{t}_R$ component of the [light] $\tilde{t}_1$ wave-function by $\cos\theta_{\tilde{t}}$, the coefficients of the $\cos\theta$-terms

in Eqs.(2.13) are altered from unity to

$$\alpha_{\tilde{t}_{1,2}} \;=\; \pm \cos 2\theta_{\tilde{t}} \, \beta_t \, \kappa_{\tilde{t}_{1,2}}^{-1} \,, \tag{2.14}$$

$$\text{where} \quad \kappa_{\tilde{t}_{1,2}} \;=\; 1 \pm 2 \sin 2\theta_{\tilde{t}} \,(1 - \beta_t^2)^{1/2} \,,$$

and β_t is the velocity of the top quark in the gluino rest frame. As expected, non-zero top mass and mixing dilute the polarization effects.

As discussed previously, the spin information is washed out in inclusive analyses of the final states. Adding up quarks/antisquarks and antiquarks/squarks, the $\cos\theta$-dependent terms cancel each other. These final states can be discriminated however by tagging either the charge of the quark/antiquark t, b in the third generation, or by tagging the squark/antisquark by measuring the charges in chargino decays. This method can successfully be applied within the first [second] generation only if up- and down-states can be distinguished since the states $\tilde{u}_L$ and $\tilde{d}_L^*$ generate final states with the same charge topology but opposite quark/antiquark helicities. If, however, their decay branching ratios are different, the spin-dependent contributions of the two channels do not add up to zero anymore but come with the spin analysis power $\kappa = |BR_{\tilde{d}} - BR_{\tilde{u}}|/[BR_{\tilde{d}} + BR_{\tilde{d}}] \neq 0$. Though the partial widths for decays to charginos are the same by isospin invariance, the total widths of $\tilde{u}$ and $\tilde{d}/\tilde{d}^*$ may be different, nevertheless, for $\tilde{\chi}_2^0$ and $\tilde{\chi}_1^0$ not being pure wino and bino states [20].

2.3. Bypass: The Dirac Alternative

If the gluinos were Dirac particles [8] as formulated in N=2 hybrid models, they could only be produced in the fermion-antifermion mode of gluino-pair production:

$$q\bar{q}, \; gg \;\rightarrow\; \tilde{g}_D \tilde{g}_D^c \,. \tag{2.15}$$

The decay channels would be restricted, by conservation of the Dirac charge, to

$$\tilde{g}_D \;\rightarrow\; \bar{q}_L \tilde{q}_R \quad \text{and} \quad q_L \tilde{q}_L^* \tag{2.16}$$

$$\tilde{g}_D^c \;\rightarrow\; \bar{q}_R \tilde{q}_L \quad \text{and} \quad q_R \tilde{q}_R^* \,. \tag{2.17}$$

Assuming, as done commonly, the $\tilde{q}_R, \tilde{q}_R^*$ squarks to decay into the lightest, invisible neutralino $\tilde{\chi}_1^0 = $ LSP, and tagging the $\tilde{q}_L, \tilde{q}_L^*$ squarks, the spins of the *individual* gluinos $\tilde{g}$ and $\tilde{g}^c$ can be reconstructed with spin-analysis power 1 in the Dirac theory. Unlike the Majorana theory, quark and antiquark always come with opposite helicities in pairs.

2.4. Spin-Phenomenology of Gluino-Pair Production

The spin-correlation effects in gluino-pair production will be illustrated by the analysis of jet-jet invariant masses as a simple indicator. Since spin correlations will play only a rôle in precision measurements at LHC, our illustration is designed to be of qualitative theoretical nature, without cuts on observables and QCD radiative corrections, *etc.* Thus, only a coarse picture of spin effects will be presented for illustration as [semi]realistic experimental simulations are far beyond the scope of this theoretical study.

Quite generally, spin correlation effects are described in the process $pp \rightarrow \tilde{g}\tilde{g} \rightarrow final\ state$ by the production correlation matrix $\mathcal{C}$ and the two decay polarization vectors $\mathcal{P}_1$ and $\mathcal{P}_2$ [15]:

$$d\sigma = d\sigma^{\text{unpol}} \left[1 + \mathcal{C}_{\mu\nu} \mathcal{P}_{1\mu} \mathcal{P}_{2\nu} \right] . \tag{2.18}$$

The spin correlation affects in principle all final-state observables.

The decay chains of the two gluinos, cf. Fig. 4,

$$\tilde{g}_1 \tilde{g}_2 \;\rightarrow\; [\bar{q}_1 \tilde{q}_1] \, [\bar{q}_2 \tilde{q}_2] \rightarrow \bar{q}_1 q_1 \bar{q}_2 q_2 \, \tilde{\chi}\tilde{\chi} \tag{2.19}$$
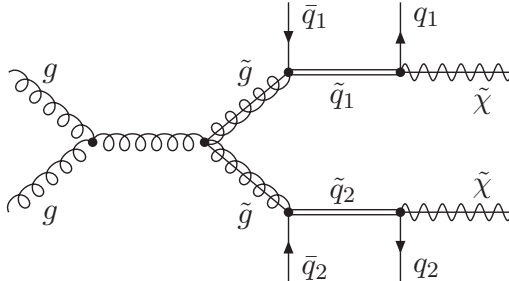
FIG. 4: Squark decay chain in gluino-pair production; chains involving anti-squarks are to be added.

give rise to six invariant masses $M_{ij}^2 = (p_i + p_j)^2$ which can be formed within the four-jet ensemble of the final state.

The invariant mass distribution of the two near-jets, labeled generically by $\bar{q}_1$ and $\bar{q}_2$, is most sensitive to the gluino polarization. While it will not be known in practice which of the observed final-state jets are associated with the near-jets in the gluino decays, in the vast majority of events for SPS1a/a′-type mass configurations these two jets can be identified with the jets of minimal transverse momentum. Ordering therefore the jets j_1 to j_4 according to rising transverse momenta, the $j_1 j_2$ combination is expected to retain most of the sensitivity to spin correlations. Note that for gluino Majorana theories the $\bar{q}_1 \bar{q}_2$ combination comes in all possible configurations: $\bar{q}_R \tilde{q}_L$ with $\bar{q}_R \tilde{q}_L$ and $q_L \tilde{q}_L^*$, i.e. equal-helicity as well as opposite-helicity (anti)quark states generating the low-$p_\perp$ jets. In contrast, Dirac theories would only allow opposite-helicity (anti)quark states generating these jets.

To illustrate the effect of spin correlations we compare the jet-jet invariant mass distributions for $\tilde{u}_L \tilde{u}_L$ and $\tilde{u}_L \tilde{u}_L^*$ intermediate states, associated with $\bar{q}_R \bar{q}_R$ and $\bar{q}_R q_L$ near-quark jets. The L squarks $\tilde{u}_L, \tilde{u}_L^*$ can be tagged by observing leptonic decays of $\tilde{\chi}_1^\pm$ and $\tilde{\chi}_2^0$, which discriminate L squarks from R squarks decaying to the invisible $\tilde{\chi}_1^0$, cf. Ref. [8]. By tagging the L squarks, kinematical effects due to different L/R squark masses, with size similar to the spin effects, are eliminated. The spin-correlations will manifest themselves in different values of the jet-jet invariant masses, which depend on the relative orientation of the gluino spins. The average values $\langle M^2 \rangle = (\langle M_{\tilde{u}_L \bar{u}_L}^2 \rangle + \langle M_{\tilde{u}_L \bar{u}_L^*}^2 \rangle)/2$ and the differences $\Delta M^2 = |\langle M_{\tilde{u}_L \bar{u}_L}^2 \rangle - \langle M_{\tilde{u}_L \bar{u}_L^*}^2 \rangle|$ [the indices characterizing the intermediate squarks] are presented in Table I for all six jet-jet invariant masses. The numerical results have been obtained for the SPS1a′ scenario with masses $M_{\tilde{g}} = 607$ GeV, $M_{\tilde{u}_L} = 565$ GeV, and $M_{\tilde{\chi}} = M_{\tilde{\chi}_1^0} = 98$ GeV. The CTEQ6L1 LO parton densities [21] have been adopted with the corresponding leading-order α_s, and all scales have been set to $\mu = M_{\tilde{g}}$. All numerical results presented in this section and below have been compared with results obtained using MadGraph/MadEvent [22]; the results do agree with each other.

In the upper section of Table I invariant masses for identified jets are shown, and in the lower section for jets ordered according to transverse momenta. For the SPS1a/a′-type mass configurations considered here, the invariant mass distributions involving near jets from the $\tilde{g} \to q\tilde{q}$ decays are significantly softer than those involving far jets from $\tilde{q} \to q\tilde{\chi}$ decays. The gluino polarization affects the invariant mass distribution involving the near jets, with a relative difference between $\tilde{u}_L \tilde{u}_L$ and $\tilde{u}_L \tilde{u}_L^*$ intermediate states of about 10%. For all other invariant mass combinations the polarization effects are negligible. As evident from the lower section of the table, the average invariant mass and the invariant mass difference for the two jets with the smallest transverse momentum $j_1 j_2$ are very close to the corresponding $\bar{q}_1 \bar{q}_2$ jet values, in concordance with general expectations derived from the kinematics associated with $\tilde{q}, \tilde{g}$ mass parameters chosen in this example.

The differential distribution of the $p_\perp$-ordered jet-jet invariant mass $M_{j_1 j_2}^2$ is depicted in Fig. 5(a) for constructive spin-correlation and contrasted with destructive correlation. Correlations among jets generated almost exclusively in scalar squark decays are tiny as evident from the $M_{j_3 j_4}^2$ distributions shown in Fig. 5(b). Without working out the details it should be noted that cuts on the minimal missing energy could be used to eliminate standard QCD stray jets. Lower $p_\perp$ cuts of order 50 GeV suppress additional QCD brems-strahl jets emitted in the supersymmetric parton process itself; estimates indicate that the signal of the spin-correlations is reduced by some 50% when the cuts are applied.

Gluino pairs:$\tilde{g}\tilde{g} \to [\bar{q}\tilde{q}][\bar{q}\tilde{q}] \to \bar{q}_1 q_1 \bar{q}_2 q_2 \tilde{\chi}\tilde{\chi}$						
original quarks	$\bar{q}_1 q_1$	$\bar{q}_1 \bar{q}_2$	$\bar{q}_1 q_2$	$q_1 \bar{q}_2$	$q_1 q_2$	$\bar{q}_2 q_2$
$\langle M^2 \rangle$ [10^3 GeV^2]	23.9	9.17	62.4	62.2	423	23.9
$\Delta M^2/\langle M^2 \rangle$ [%]	<0.1	10.8	0.8	0.8	<0.1	<0.1
$p_\perp$ ordered jets	$j_1 j_2$	$j_1 j_3$	$j_1 j_4$	$j_2 j_3$	$j_2 j_4$	$j_3 j_4$
$\langle M^2 \rangle$ [10^3 GeV^2]	9.56	30.1	43.7	39.6	64.7	417
$\Delta M^2/\langle M^2 \rangle$ [%]	10.2	2.4	1.7	2.0	3.0	<0.1

TABLE I: Invariant jet-jet masses for gluino-pair production and decay. The average values $\langle M^2 \rangle$ and the differences ΔM^2 of the invariant mass distributions for $\tilde{u}_L \tilde{u}_L$ and $\tilde{u}_L \tilde{u}_L^*$ intermediate states are shown for identified jets (upper section) and for jets ordered according to transverse momenta (lower section).
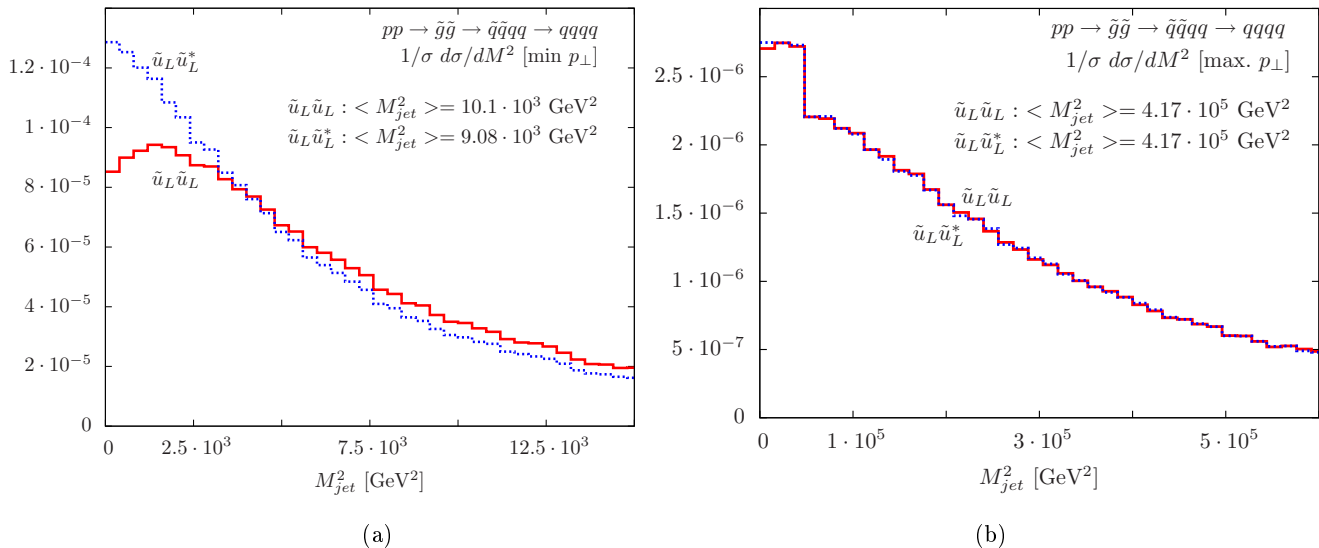

(a)   (b)

FIG. 5: Mass distribution of (a) the two jets with the lowest $p_\perp$, for which maximal spin correlations are predicted, and (b) the two jets with the highest $p_\perp$ where spin effects, within quark pairs generated almost exclusively by scalar decays, are expected to be very small.

3.   SUPER-COMPTON PROCESS

3.1.   Parton Level

Single polarization in gluino pair-production has been proved in the foregoing section to be strongly suppressed at the squark-mass level $\sim |M_L^2 - M_R^2|/[M_L^2 + M_R^2]$ for the two light generations since the production process becomes effectively parity-even in the limit $M_L \to M_R$. However, if the squarks are produced as final particles, the L/R character can be identified and the parity-violation in the Yukawa vertex becomes effective. For example, R-squarks may decay into the invisible LSP while L-squarks can be marked by chargino decays. This constellation is realized in the super-Compton process Eq. (1.3).

Symmetrizing $qg \oplus gq$ as relevant for parton collisions at the symmetric pp collider LHC, the spin-summed total

cross section [4, 5, 23] may be written

$$\sigma[qg \to \tilde{q}_{R,L}\tilde{g}] = \frac{\pi\alpha_s\hat{\alpha}_s}{s} \left[\left(1 + \frac{m_-^2}{2} - \frac{m_{\tilde{q}}^2 m_-^2}{8} \right) L_+ + \left(\frac{2m_-^2}{9} - \frac{m_{\tilde{q}}^2 m_-^2}{8} - \frac{m_-^4}{18} \right) L_- \right.$$
$$\left. -p \left(\frac{7}{9} + \frac{32m_-^2}{9} \right) \right] \tag{3.1}$$

with

$$L_{\pm} = \log \frac{1 + p \pm m_-^2/4}{1 - p \pm m_-^2/4}, \tag{3.2}$$

while the angular dependence reads:

$$\frac{d\sigma}{d\Omega}[qg \to \tilde{q}_{R,L}\tilde{g}] = \frac{\alpha_s\hat{\alpha}_s\, p}{s} \left[\frac{1}{36}\,\kappa_{\tilde{g}-} - \frac{1}{36\kappa_{\tilde{q}+}^2}(m_{\tilde{q}}^2 - \kappa_{\tilde{q}+})(m_-^2 + 2\kappa_{\tilde{q}+}) \right.$$
$$- \frac{1}{16\,\kappa_{\tilde{g}-}^2} \left[m_{\tilde{g}}^2(m_-^2 - 2\kappa_{\tilde{g}-}) - 2\kappa_{\tilde{g}-}(\kappa_{\tilde{g}-} + \kappa_{\tilde{q}+}) \right]$$
$$+ \frac{1}{576\,\kappa_{\tilde{q}+}} \left[m_-^4 - 2(m_{\tilde{g}}^2 + m_{\tilde{q}}^2) + 2\kappa_{q+}(m_-^2 + 2) \right]$$
$$+ \frac{1}{64\,\kappa_{\tilde{g}-}} \left[m_{\tilde{g}}^4 - 2m_{\tilde{g}}^2(m_{\tilde{q}}^2 + \kappa_{\tilde{g}-}) + (m_{\tilde{q}}^2 - 4)(m_{\tilde{q}}^2 + 2\kappa_{\tilde{g}-}) \right]$$
$$\left. + \frac{1}{32\,\kappa_{\tilde{q}+}\kappa_{\tilde{g}-}} \left[m_{\tilde{q}}^4 - m_{\tilde{g}}^4 + \kappa_{\tilde{g}-}(m_{\tilde{q}}^2 + m_{\tilde{g}}^2) - 2\kappa_{\tilde{q}+}(m_{\tilde{g}}^2 + \kappa_{\tilde{g}-}) \right] \right]^{\mathcal{S}}, \tag{3.3}$$

where the abbreviations

$$\kappa_{\tilde{q}\pm} = \epsilon_{\tilde{q}}(1 \pm \beta_{\tilde{q}}\cos\theta) \tag{3.4}$$

and

$$m_{\tilde{q}} = 2M_{\tilde{q}}/\sqrt{s} \qquad\qquad \epsilon_{\tilde{q}} = 2E_{\tilde{q}}/\sqrt{s} = 1 + (m_{\tilde{q}}^2 - m_{\tilde{g}}^2)/4$$
$$\beta_{\tilde{q}} = p/\epsilon_{\tilde{q}} \qquad\qquad p = \sqrt{[1 - (m_{\tilde{q}} + m_{\tilde{g}})^2/4]\,[1 - (m_{\tilde{q}} - m_{\tilde{g}})^2/4]} \tag{3.5}$$

have been used; $\tilde{q} \Leftrightarrow \tilde{g}$ correspondingly. These spin-averaged cross sections, discussed in detail in Ref. [5], are form-identical for $\tilde{q}_L$ and $\tilde{q}_R$ production.

The polarization vector of the gluino,

$$\frac{d\sigma(s)}{d\Omega} = \frac{d\sigma}{d\Omega} \frac{1}{2} \left[1 - \mathcal{C}_\mu s^\mu \right], \tag{3.6}$$

using the spin-vector notation within the frame introduced before, can easily be determined:

$$\mathcal{C}_\mu = \frac{\alpha_s\hat{\alpha}_s\, p\, m_{\tilde{g}}}{s} \left[-\frac{1}{36}k_{1\mu} + \frac{1}{8\,\kappa_{\tilde{g}-}^2} \left((\kappa_{\tilde{g}+} - 2)k_{1\mu} + (m_{\tilde{g}}^2 - \kappa_{\tilde{g}-})k_{2\mu} \right) \right.$$
$$+ \frac{1}{72\,\kappa_{\tilde{q}+}^2} \left[m_{\tilde{g}}^2 + m_{\tilde{q}}^2 - 2(p^2 - \epsilon_{\tilde{q}}^2 + 2(1 + p\cos\theta)) \right] k_{2\mu}$$
$$- \frac{1}{32\,\kappa_{\tilde{g}-}} \left[(\kappa_{\tilde{g}+} - 4)k_{1\mu} + (\kappa_{\tilde{g}+} - 2\epsilon_{\tilde{q}})k_{2\mu} \right]$$
$$- \frac{1}{576\,\kappa_{\tilde{q}+}} \left[2(2 + p\cos\theta - \epsilon_{\tilde{q}})k_{1\mu} + 2(4 - 3\epsilon_{\tilde{q}} + p\cos\theta)k_{2\mu} \right]$$
$$\left. + \frac{1}{32\,\kappa_{\tilde{g}-}\kappa_{\tilde{q}+}} \left[2(2 + p\cos\theta - \epsilon_{\tilde{q}})k_{1\mu} + 2(m_{\tilde{g}}^2 - p^2 + \epsilon_{\tilde{q}}^2)k_{2\mu} \right] \right]^{\mathcal{S}} /\mathcal{N}_{qg}. \tag{3.7}$$
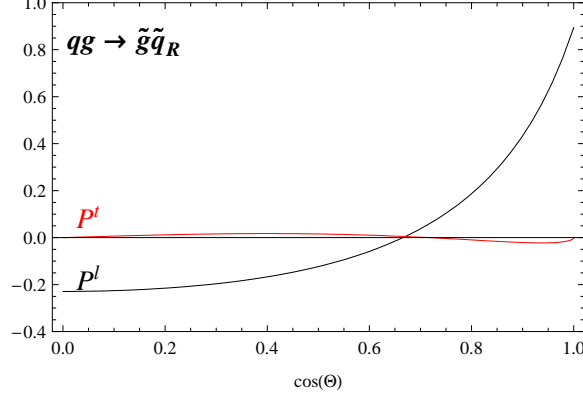
FIG. 6: Longitudinal and transverse components of the gluino polarization vector for R-squarks in the final state of the super-Compton process.

$\mathcal{N}_{qg}$ denotes the symmetrized angular distribution Eq.(3.3). Evaluation of the vector in the gluino rest frame yields the final results for the longitudinal, transverse and normal components:

$$
\begin{aligned}
\mathcal{P}^l \;=\;& \frac{\alpha_s \hat{\alpha}_s\, p}{s} \left[\frac{1}{36}(\epsilon_{\tilde{g}} \cos\theta - p) + \frac{1}{8\,\kappa_{\tilde{g}_-}^2} \left[(2\epsilon_{\tilde{g}} - \epsilon_{\tilde{q}}\, m_{\tilde{g}}^2) \cos\theta + p\,(m_{\tilde{g}}^2 - 2) \right] \right. \\[2mm]
& - \frac{1}{72\,\kappa_{\tilde{q}_+}^2} \left[(p + \epsilon_{\tilde{g}} \cos\theta)(3\,(2\epsilon_{\tilde{g}} - m_{\tilde{g}}^2) - (2\epsilon_{\tilde{q}} + m_{\tilde{q}}^2) + 4p\cos\theta) \right] \\[2mm]
& - \frac{1}{16\,\kappa_{\tilde{g}_-}} \left[(p^2 + \epsilon_{\tilde{g}}^2)\cos\theta - 2p\epsilon_{\tilde{q}} \right] - \frac{1}{288\,\kappa_{\tilde{q}_+}} \left[2\,(p^2 + \epsilon_{\tilde{g}}(1 - \epsilon_{\tilde{q}}))\cos\theta + 2p\,(3 - 2\epsilon_{\tilde{g}}) \right] \\[2mm]
& \left. - \frac{1}{16\,\kappa_{\tilde{q}_+}\kappa_{\tilde{g}_-}}[\epsilon_{\tilde{g}}\, p \cos^2\theta - \frac{p}{4}(5m_{\tilde{g}}^2 + 3m_{\tilde{q}}^2 + 4) + \frac{1}{4}\,(m_{\tilde{q}}^4 - m_{\tilde{g}}^4 - 4m_{\tilde{q}}^2)\cos\theta \right]^{\mathcal{S}} /\mathcal{N}_{qg} \\[4mm]
\mathcal{P}^t \;=\;& \frac{\alpha_s \hat{\alpha}_s\, p\, m_{\tilde{g}}\,\sin\theta}{s} \left[\frac{1}{8\,\kappa_{\tilde{g}_-}^2} \left[2(\epsilon_{\tilde{g}} - 1) - m_{\tilde{g}}^2 \right] - \frac{1}{72\,\kappa_{\tilde{q}_+}^2} \left[3(m_{\tilde{g}}^2 - 2\epsilon_{\tilde{g}}) + (m_{\tilde{q}}^2 + 2\epsilon_{\tilde{q}}) - 4p\cos\theta \right] \right. \\[2mm]
& \left. + \frac{\epsilon_{\tilde{g}}}{16\,\kappa_{\tilde{g}_-}} + \frac{\epsilon_{\tilde{g}} - \epsilon_{\tilde{q}}}{288\,\kappa_{\tilde{q}_+}} - \frac{1}{16\,\kappa_{\tilde{q}_+}\kappa_{\tilde{g}_-}} \left[2(m_{\tilde{g}}^2 - 2\epsilon_{\tilde{g}}) + \epsilon_{\tilde{q}} + 2 - p\cos\theta \right] \right]^{\mathcal{A}} /\mathcal{N}_{qg} \\[4mm]
\mathcal{P}^n \;=\;& 0
\end{aligned}
\tag{3.8}
$$

at the Born level for R-squarks in the final state, while the overall signs flip for L-squarks. The non-trivial longitudinal and transverse components of the polarization vector are displayed in Fig. 6 for the parton invariant energy $\sqrt{s} = 2$ TeV and the SPS1a′ masses $M_{\tilde{g}} = 607$ GeV and $M_{\tilde{q}} = M_{\tilde{u}_R} = 547$ GeV. While the transverse polarization is very small for all production angles, the maximal parity violation of the Yukawa vertex renders the degree of longitudinal polarization large in the forward direction.

Normal gluino polarization is zero in Born approximation, but it can be generated by vertex loop-corrections which render the transition matrix formally T-odd. For example, the triangular $\tilde{q}\tilde{g}g$ super-QCD vertex correction to the amplitude $gq \to \tilde{g}\tilde{q}$ is complex, but the size of the normal polarization remains suppressed as a higher-order effect [15] at a level of $\alpha_s \tilde{M}/\sqrt{s}$, with $\tilde{M}$ denoting the typical supersymmetry mass scale.

The Dirac theory would generate, in the restricted set of processes $qg \to \tilde{q}_R \tilde{g}_D^c$ and $\tilde{q}_L \tilde{g}_D$, the same degree of polarization.

The single polarization vector can be determined experimentally by using the two methods discussed in the previous section:

(a) Tagging of the $\tilde{u}_L, \tilde{d}_L^*$ or $\tilde{d}_L, \tilde{u}_L^*$ squarks by searching for ℓ^+ or ℓ^- final states allows to reconstruct the spin with analysis power $\kappa = |BR_{\tilde{d}} - BR_{\tilde{u}}|/[BR_{\tilde{d}} + BR_{\tilde{d}}]$ in the first two generations.
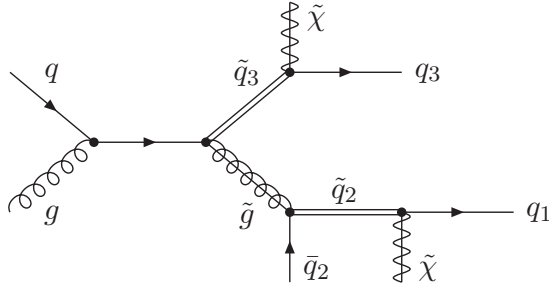
FIG. 7: Decay chains in the super-Compton process. While q is effectively restricted to valence u, d quarks, the squark $\tilde{q}_2$ may be substituted by the corresponding anti-squark, the attached [anti]quarks correspondingly.

(b) Analysis of stop and sbottom final states allows the reconstruction of the spin vector, without dilution by destructive interference effects of different flavors but with some dilution due to the superposition of near and far-top quarks.

3.2. Spin-Phenomenology of the Super-Compton Process

The spin effects in the super-Compton process are described by the polarization vectors $\mathcal{C}_\mu$ and $\mathcal{P}_\mu$ in the gluino production and decay processes [15]:

$$d\sigma = d\sigma^{\text{unpol}}[1 - \mathcal{C}_\mu \mathcal{P}_\mu]. \tag{3.9}$$

Depending on the sign of the product of the production and decay polarization vectors either constructive or destructive spin effects are generated, affecting, in principle, all experimental observables.

In parallel to the foregoing gluino-pair discussion we illustrate the spin phenomenology in the super-Compton process again by analyzing jet-jet invariant masses. The reference jet will be the primary squark decay jet q_3 recoiling against the gluino decay antiquark jet $\bar{q}_2$ and the secondary quark decay jet q_1 emitted in the squark decay of the gluino chain, cf. Fig. 7:

$$\tilde{q}\tilde{g} \to [\tilde{q}_3]\,[\bar{q}_2\tilde{q}_2] \to q_3\bar{q}_2 q_1 \tilde{\chi}\tilde{\chi}. \tag{3.10}$$

The incoming quarks will be taken as u, d valence quarks. Three invariant masses $q_1\bar{q}_2, q_1q_3, \bar{q}_2q_3$ can be formed from the three final-state quark momenta. Since the polarization vector $\mathcal{P}$ can be varied by picking L squarks or antisquarks in the $\tilde{g}$ decay state, different values are predicted for the jet-jet invariant masses.

Gluino Majorana theories generate equal- and opposite-helicity (anti)quark final states $\bar{q}_2q_3$ while Dirac theories restrict these final states to equal-helicity pairs.

The average values of the three jet-jet invariant masses for $\tilde{u}_L\tilde{u}_L$ and $\tilde{u}_L\tilde{u}_L^*$ final states coming with u_L and $u_L/\bar{u}_R$ quark jets are presented in Tab.II, for identified jets in the upper row, and jet pairs ordered according to rising invariant masses M_{inv} in the second row.

As evident from the table, the combination $\bar{q}_2q_3$, involving the primary antiquark decay jet of the polarized gluino, provides the highest sensitivity to spin effects. This combination is mapped, on the average, to the second largest invariant mass in the M_{inv} ordered three-jet ensemble. A clear distinction emerges between constructive and destructive spin effects in this observable. If large invariant masses for the three-jet final states are selected, say $M_{jjj} > 2.5$ TeV, the longitudinal gluino polarization is greatly enlarged, boosting forward or backward the recoiling decay squark, and raising or lowering the jet-jet invariant masses accordingly. The spin-dependent distributions of the second largest invariant mass are depicted in Fig. 8(a). [The contamination due to same-side $\bar{q}_2q_1$ partons, which generate the wedge with the standard sharp edge at $\approx [M_{\tilde{g}}^2 - M_{\tilde{q}}^2]$ but do not give rise to spin asymmetries, is subtracted for illustration in the two lower curves.] Correlations among squark decay jets $[q_1q_3]$ are small, Fig. 8(b), as expected.

Super-Compton:$\tilde{q}\tilde{g} \to [\tilde{q}][\bar{q}\tilde{q}] \to q_3\bar{q}_2q_1\,\tilde{\chi}\tilde{\chi}$			
original quarks	$q_1\bar{q}_2$	q_1q_3	$\bar{q}_2q_3$
$\langle M^2 \rangle$ [10^4 GeV^2]	2.39	48.3	7.13
$\Delta M^2/\langle M^2 \rangle$ [%]	<0.1	0.8	7.9
M_{inv} ordered jets	small	medium	large
$\langle M^2 \rangle$ [10^4 GeV^2]	1.80	7.33	48.7
$\Delta M^2/\langle M^2 \rangle$ [%]	5.0	5.9	0.7
$M_{\mathrm{jjj}} > 2.5$ TeV :	small	medium	large
$\langle M^2 \rangle$ [10^4 GeV^2]	2.46	76.3	775
$\Delta M^2/\langle M^2 \rangle$ [%]	10.3	21.2	2.0

TABLE II: Invariant jet-jet masses in the super-Compton process. The average values $\langle M^2 \rangle$ and the differences ΔM^2 of the invariant mass distributions for $\tilde{u}_L\tilde{u}_L$ and $\tilde{u}_L\tilde{u}_L^*$ intermediate states are shown for identified jets (upper section) and for jets ordered according to invariant mass (middle section). The lower section shows the enhanced polarization effects if large invariant masses $M_{jjj} > 2.5$ TeV are selected.
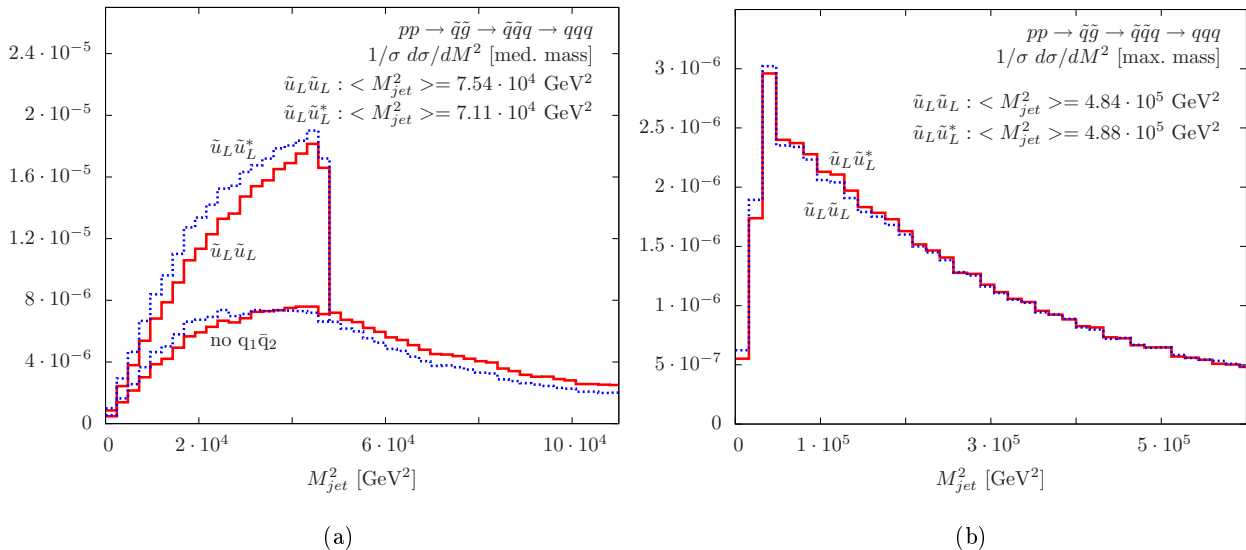

(a)   (b)

FIG. 8: Mass distribution of (a) the second largest invariant mass; the same-side $q_1\bar{q}_2$ parton combination is subtracted in the lower curves; (b) the distribution for jets of maximal invariant mass, corresponding largely to partons q_1q_3.

4. SUMMARY

Spin correlations in gluino-pair production and polarization effects in single gluino production of the super-Compton process affect the distributions of the experimentally observed final states. In this report we have analyzed the theoretical basis of these effects, calculating the two-gluino spin-correlation matrix in the first case and the gluino polarization vector in the second. A few examples for jet invariant masses illustrate the size of these effects at the theoretical level. They become relevant only if L and R squarks, coming in association with R/L polarized antiquarks, *etc.*, are discriminated by measuring, for instance, charges in the third generation. The spin effects are modest, typically of about 10% in the spin-sensitive observables. Nevertheless, when the LHC potential is fully exploited for precision measurements and analyses are performed to determine supersymmetry parameters like mixings, couplings, *etc.*, such effects must be controlled properly in the analyses of the measured final states. The report is intended to provide a first step in this direction.

Acknowledgments

---

[1] Yu. A. Golfand and E. P. Likhtman, JETP Lett. **13** (1971) 3214; J. Wess and B. Zumino, Nucl. Phys. B **70** (1974) 39.

[2] H. P. Nilles, Phys. Rept. **110** (1984) 1; H. E. Haber and G. L. Kane, Phys. Rept. **117** (1985) 75.

[3] J. Wess and J. Bagger, *Princeton, USA: Univ. Pr. (1992) 259 p*; P. Binetruy, "Supersymmetry: Theory, experiment and cosmology," *Oxford, UK: Oxford Univ. Pr. (2006) 520 p*; M. Drees, R. Godbole and P. Roy, "Theory and phenomenology of sparticles: An account of four-dimensional N=1 supersymmetry in high energy physics," *Hackensack, USA: World Scientific (2004) 555 p*.

[4] S. Dawson, E. Eichten and C. Quigg, Phys. Rev. D **31** (1985) 1581.

[5] W. Beenakker, R. Höpker, M. Spira and P. M. Zerwas, Nucl. Phys. B **492** (1997) 51 [arXiv:hep-ph/9610490].

[6] A. J. Barr, Phys. Lett. B **596** (2004) 205 [arXiv:hep-ph/0405052]; J. M. Smillie and B. R. Webber, JHEP **0510** (2005) 069 [arXiv:hep-ph/0507170]; A. Alves, O. Eboli and T. Plehn, Phys. Rev. D **74** (2006) 095010 [arXiv:hep-ph/0605067]; C. Csaki, J. Heinonen and M. Perelstein, JHEP **0710** (2007) 107 [arXiv:0707.0014 [hep-ph]].

[7] B. C. Allanach *et al.*, "The Snowmass points and slopes: Benchmarks for SUSY searches," *in* Proc. of the APS/DPF/DPB Summer Study on the Future of Particle Physics, Snowmass (Colorado) 2001, and Eur. Phys. J. C **25** (2002) 113 [arXiv:hep-ph/0202233]; J. A. Aguilar-Saavedra *et al.*, Eur. Phys. J. C **46** (2006) 43 [arXiv:hep-ph/0511344].

[8] S. Y. Choi, M. Drees, A. Freitas and P. M. Zerwas, Phys. Rev. D **78** (2008) 095007 [arXiv:0808.2410 [hep-ph]].

[9] M. M. Nojiri and M. Takeuchi, Phys. Rev. D **76** (2007) 015009 [arXiv:hep-ph/0701190].

[10] P. Fayet, Nucl. Phys. B **113** (1976) 135; L. Álvarez-Gaumé and S. F. Hassan, Fortsch. Phys. **45** (1997) 159 [arXiv:hep-th/9701069]; K. Benakli and C. Moura, *in* M. M. Nojiri *et al.*, arXiv:0802.3672 [hep-ph].

[11] S. Y. Choi, M. Drees, J. Kalinowski, J. M. Kim, E. Popenda and P. M. Zerwas, Phys. Lett. B **672** (2009) 246 [arXiv:0812.3586 [hep-ph]]; T. Plehn and T. M. P. Tait, arXiv:0810.3919 [hep-ph] and revised version.

[12] S. Y. Choi, K. Hagiwara, Y. G. Kim, K. Mawatari and P. M. Zerwas, Phys. Lett. B **648** (2007) 207 [arXiv:hep-ph/0612237].

[13] A. Kulesza and L. Motyka, arXiv:0807.2405 [hep-ph].

[14] E. Popenda, *Diploma Thesis*, Institut für Theoretische Physik, RWTH Aachen, March 2009.

[15] J. H. Kühn, A. Reiter and P. M. Zerwas, Nucl. Phys. B **272** (1986) 560.

[16] W. Bernreuther, A. Brandenburg, Z. G. Si and P. Uwer, Nucl. Phys. B **690** (2004) 81 [arXiv:hep-ph/0403035].

[17] W. Beenakker, R. Höpker and P. M. Zerwas, Phys. Lett. B **378** (1996) 159 [arXiv:hep-ph/9602378];

[18] M. Mühlleitner, A. Djouadi and Y. Mambrini, Comput. Phys. Commun. **168** (2005) 46 [arXiv:hep-ph/0311167].

[19] W. Beenakker, R. Hopker, T. Plehn and P. M. Zerwas, Z. Phys. C **75** (1997) 349 [arXiv:hep-ph/9610313].

[20] A. Freitas, P. Z. Skands, M. Spira and P. M. Zerwas, JHEP **0707** (2007) 025 [arXiv:hep-ph/0703160].

[21] J. Pumplin, D. R. Stump, J. Huston, H. L. Lai, P. M. Nadolsky and W. K. Tung, JHEP **0207** (2002) 012 [arXiv:hep-ph/0201195].

[22] H. Murayama, I. Watanabe and K. Hagiwara, preprint KEK-91-11; T. Stelzer and W. F. Long, Comput. Phys. Commun. **81** (1994) 357 [arXiv:hep-ph/9401258]; F. Maltoni and T. Stelzer, JHEP **0302** (2003) 027 [arXiv:hep-ph/0208156]; J. Alwall, P. Artoisenet, S. de Visscher, C. Duhr, R. Frederix, M. Herquet and O. Mattelaer, AIP Conf. Proc. **1078** (2009) 84 [arXiv:0809.2410 [hep-ph]].

[23] W. Hollik, E. Mirabella and M. K. Trenkel, JHEP **0902** (2009) 002 [arXiv:0810.1044 [hep-ph]].